PAPER

Check for updates

Theoretical insights of silicene doped with transition metals as C – reactive protein biosensors for cardiac vascular applications using density functional theory

Kalpana Devi P,[a] Aiswarya T,[a] K. K. Singh,[a] Vilas H. Gaidhane[b] and Neeru Sood [c]

Early and accurate detection of C-reactive protein (CRP), a key biomarker for inflammation and cardiovascular conditions, remains a critical need in medical diagnostics. In this study, we employ density functional theory calculations using the B3LYP functional in Gaussian 16 to explore the CRP sensing potential of silicene doped with iron and nickel atoms at central and edge sites. Using density functional theory with the B3LYP functional in Gaussian 16, we systematically analyze the adsorption behavior, thermodynamic stability, and electronic response of CRP-bound systems. Adsorption energy and thermodynamic parameters confirm spontaneous and exothermic interactions, with the iron doped at center configuration exhibiting the strongest adsorption and highest charge transfer. The interaction of CRP induces pronounced changes in the electronic structure, including energy gap modulation, Fermi level shifts, and enhanced density of states near the Fermi level, indicating improved electronic sensitivity. Comparative analysis shows that the nickel doped at edge configuration also exhibits significant responsiveness, with an adsorption energy and energy gap change. Furthermore, non-covalent interaction plots reveal strong van der Waals interactions between CRP and the doped silicene surfaces, confirming favorable adsorption mechanisms. These combined insights from electronic structure, thermodynamic, and interaction analyses establish that the iron doped at center of silicene and nickel doped at edge of silicene configurations might act as promising candidates for next-generation CRP biosensors based on two-dimensional materials.

Introduction

Cardiovascular diseases (CVDs) continue to be the primary cause of death globally, highlighting the need for the creation of sophisticated diagnostic instruments to identify and track them at an early stage. Out of all the biomarkers, C-reactive protein (CRP) has become recognized as a prominent predictor of inflammation linked to cardiovascular problems.[1] Higher levels of CRP are directly associated with a greater risk of heart attack, stroke, and peripheral artery disease, making it an essential target for bio-sensing applications.[2] Biosensors, which combine biological recognition elements with physicochemical transducers, provide a promising method for quickly and accurately detecting biomarkers such as CRP. These devices convert the biological interaction between the target molecule and the recognition element into a detectable signal, making it easier to monitor disease conditions in real time.[3,4] A dependable biosensor for CRP detection could greatly improve the diagnosis and treatment of cardiovascular illnesses, allowing for prompt intervention and better patient results.

Nanotechnology has rapidly transformed the field of biosensing by providing remarkable sensitivity and selectivity in detecting biomolecules.[5,6] 2D materials have attracted considerable interest due to their distinct electrical, mechanical, and chemical capabilities, among other nanoparticles.[7,8] Silicene, a single layer of silicon atoms structured in a honeycomb lattice-like graphene, has emerged as a highly promising candidate for biosensing applications.[9–11] Silicene possesses numerous favourable features that render it well-suited for biosensing applications. The sensor's sensitivity is enhanced by the abundant opportunities for biomolecule interaction due to its large surface area.[12] Furthermore, the distinctive electrical characteristics of silicene, such as its adjustable bandgap and exceptional carrier mobility, enable the creation of sensors that are highly sensitive and discerning.[13] Moreover, silicene exhibits compatibility with prevailing silicon-based technologies, hence

[a]Department of Physics, Birla Institute of Technology - Pilani (Dubai Campus), UAE. E-mail: kalpana@dubai.bits-pilani.ac.in; aiswarya@dubai.bits-pilani.ac.in; singh@dubai.bits-pilani.ac.in

[b]Department of Electrical and Electronics Engineering, Birla Institute of Technology - Pilani (Dubai Campus), UAE. E-mail: vhgaidhane@dubai.bits-pilani.ac.in

[c]Department of Biotechnology, Birla Institute of Technology and Science, Pilani-Dubai Campus, United Arab Emirates University, Dubai, UAE. E-mail: sood@dubai.bits-pilani.ac.in

facilitating its smooth incorporation into present electronic devices and systems.[14] Silicene is utilized in biosensing to detect a range of biological things, such as proteins, nucleic acids, and tiny compounds.[15–17] Silicene-based biosensors function by converting the interaction between the target biomolecule and the sensor surface into a detectable electrical signal. The interaction between the target analyte and silicene can cause modifications in its electrical properties, such as conductivity or capacitance. These changes can be measured and used to determine the presence and concentration of the analyte.[18]

Density Functional Theory (DFT) is a highly effective computational framework used to comprehend the electronic characteristics and molecular interactions that underlie the operation of biosensors.[19] Through the utilization of DFT, scientists can forecast and enhance the performance of biosensor elements at the atomic scale, guaranteeing exceptional sensitivity and accuracy in the detection of biomarkers.[20] This theoretical approach facilitates the logical development of biosensors, providing guidance for experimental endeavours and minimizing the need for trial-and-error commonly seen in older methodologies. In this manuscript, we present a comprehensive study on the design and analysis of a cardiac vascular biosensor utilizing CRP as the target biomarker. Employing DFT, we explore the interactions between CRP and the biosensor's recognition elements, aiming to enhance the device's performance. Our findings contribute to the growing field of biosensor technology, offering insights into the development of efficient and reliable diagnostic tools for cardiovascular health monitoring. The study of CRP sensor analysis using DFT at different doped positions reveals significant insights into the electronic properties and adsorption capabilities. DFT calculations have been employed to evaluate the effects of iron and nickel dopants at different positions (centre and peripheral) on the silicene sheet, highlighting the importance of dopant type and position in enhancing CRP sensor efficiency.

Methodology

Gaussian 16 software package was utilized to perform DFT calculations, aiming to examine the interactions between C-reactive protein and the silicene sheet doped with iron/nickel atom. The molecular structure of CRP was acquired from the Protein Data Bank (PDB) and the recognition part of the biosensor, the silicene sheet was designed, which was modified by doped with an iron/nickel atom to improve the strength of binding. Our study focused on the substitutional doping of iron and nickel atoms at both central and peripheral sites in a silicene sheet. We considered pristine silicene (P–Si), iron-doped silicene with the dopant at the center (Si–Fe–C) and at the periphery (Si–Fe–E), and nickel-doped silicene with the dopant at the center (Si–Ni–C) and at the periphery (Si–Ni–E). The CRP and the metal atom doped silicene sheet were initially optimized using the B3LYP exchange-correlation functional and LANL2DZ basis set.[21,22] Before conducting interaction investigations, optimizations were performed to guarantee that the structures were in their minimum energy conformations and were confirmed using frequency calculations performed at the

same level of accuracy and using the same basis set for determining thermochemical properties.[23]

The silicene system was constructed with a total of 96 silicon atoms and 26 hydrogen atoms. To remove the dangling bonds of these clusters, the outer edges of the all designed silicene sheets were fully saturated with hydrogen atoms. Usually, the silicon atoms at the edges of a silicene sheet have dangling bonds, which can lead to instability and increased reactivity. By saturating these dangling bonds with hydrogen atoms, the edge silicon atoms achieve a more stable electronic configuration, reducing reactivity and preventing unwanted interactions during the simulation. This model is frequently utilized in theoretical studies to effectively showcase the properties of periodic silicene monolayers.[24,25] The CRP and functionalized silicene structures were strategically positioned close to each other to stimulate the binding interaction. The values for thermal energy (E), thermal enthalpy (H), and thermal free energy (G) can be determined using the frequency keyword (freq) at a temperature of 298 K and one atmospheric pressure.[26] The Gaussian 16 software package was utilized to do calculations.[27] The binding energy (ΔE) was calculated using the formula,

$$\Delta(E/H/G)_{(CRP–M–Si)} = (E/H/G)_{(CRP–M–Si)} - (E/H/G)_{(M–Si)} - (E/H/G)_{CRP} \tag{1}$$

where, $E_{(CRP–M–Si)}$ and $E_{M–Si}$ correspond to energies of optimized geometries of iron/nickel atom doped silicene with and without CRP molecule, Furthermore, during the adsorption process, changes in Gibbs free energy (ΔG) and thermal enthalpy (ΔH) were also measured. Values were taken directly from the Gaussian frequency calculations and converted from Hartree to eV. Computations using energy gap variation were conducted to examine the electronic configuration of the biosensor both before and during the binding of CRP.[28] An analysis was conducted on the energies of the highest occupied molecular orbital (HOMO) and the lowest unoccupied molecular orbital (LUMO). The binding of CRP caused shifts in the HOMO–LUMO gap, which resulted in changes in the electronic characteristics that are important for the functionality of the sensor. In this study, NBO analysis is employed to investigate the electronic interactions between substitutionally doped silicene and CRP.[29] Both central (Si–Fe–C & Si–Ni–C) and peripheral (Si–Fe–E & Si–Ni–E) doping positions are considered to analyze how the dopant location affects charge transfer and electronic structure modifications upon CRP adsorption. By computing charge transfer (Δq) from natural population analysis, E^2 from second-order perturbation, and hybridization changes, this study aims to determine the optimal doping strategy that enhances the sensitivity of silicene-based biosensors for cardiovascular disease detection.

The frontier molecular orbital (FMO) energies, specifically the highest occupied molecular orbital (HOMO) and lowest unoccupied molecular orbital (LUMO), were calculated using the same computational parameters employed throughout the study. The energy band gap (E_g) was determined as the

difference between the LUMO and HOMO energy levels,[30] using the equation:

$$E_g = E_{LUMO} - E_{HOMO} \qquad (2)$$

When evaluating a sensor's effectiveness, electrical conductivity (σ) is an essential factor, especially when it comes to identifying target molecules like CRP. The mathematical expression representing electrical conductivity is:

$$\sigma = AT^{\frac{3}{2}}\exp\frac{-E_g}{2KT} \qquad (3)$$

where T is the absolute temperature, K is the Boltzmann's constant, E_g is the energy gap, and A is a constant (electrons per m^3 $K^{3/2}$). Higher electrical conductivity is achieved when the energy gap is narrower.[31] The adsorption of the target molecule leads to a notable change in electrical conductivity, which is crucial for ensuring accurate detection in the sensor.[32] To evaluate the influence of CRP adsorption on the electronic properties of the system, the energy gap was calculated both before and after gas adsorption, and the relative change was expressed as a percentage.

Additionally, the recovery time (τ) of a gas sensor based on metal-doped graphene was estimated using the Arrhenius-type expression:

$$\tau = v_0^{-1}\exp\left[-\frac{\Delta E}{K_B T} \right] \qquad (4)$$

where v_0 is the attempt frequency, ΔE is the adsorption energy, K_B is the Boltzmann constant, and T is the absolute temperature. According to this equation, stronger adsorption (larger ΔE) leads to a longer recovery time, and in some cases, may inhibit the desorption of molecules entirely, thereby affecting sensor performance.

In molecular adsorption studies, the characterization of non-covalent interactions (NCIs) between an adsorbate and an adsorbent is essential for understanding the driving forces behind binding, stability, and selectivity. While traditional geometric and energetic analyses provide useful insights, they often fall short in visualizing and distinguishing weak interactions such as van der Waals forces, hydrogen bonding, or π–π stacking. To address this, the Reduced Density Gradient (RDG) analysis has emerged as a widely used, visually intuitive method for identifying and characterizing NCIs based on the electron density and its derivatives. RDG analysis relies on the reduced density gradient function, which is sensitive to regions where the electron density is low and the gradient is small, the characteristic of non-covalent interactions.[33] When plotted in conjunction with the sign of the second eigenvalue of the Hessian matrix of the electron density (sign ($\lambda_2)\rho$), RDG enables the differentiation between attractive (hydrogen bonding) and repulsive (steric clashes) interactions. The resulting RDG iso-surfaces and 2D scatter plots provide a clear and spatially resolved visualization of interaction regions across the adsorbate–adsorbent interface. This method is particularly valuable in adsorption studies, as it allows for the non-empirical detection of weak interactions that are often critical to adsorption strength and specificity but are not easily captured by electron density or energy-based criteria alone.

Results and discussions

C-reactive protein

CRP is a widely recognized biomarker of inflammation and is commonly used in clinical diagnostics to evaluate and track inflammatory diseases.[34] CRP is a protein composed of five identical subunits that arrange themselves in a circular configuration as shown in Fig. 1. The molecular weight of the total molecule is roughly 115 kDa, with each component weighing around 23 kDa.[35] CRP attaches to phosphocholine
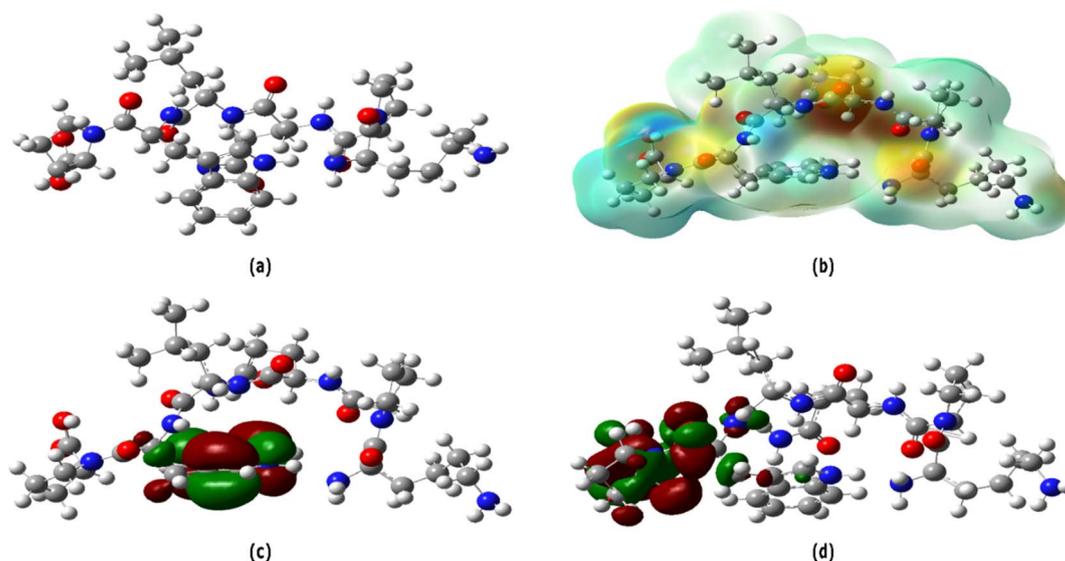

Fig. 1 (a) The structure of optimized CRP, (b) molecular electrostatic potential of CRP, (c) HOMO maps of CRP, and (d) LUMO maps of CRP (All figures in this article are available in color in the online version.).
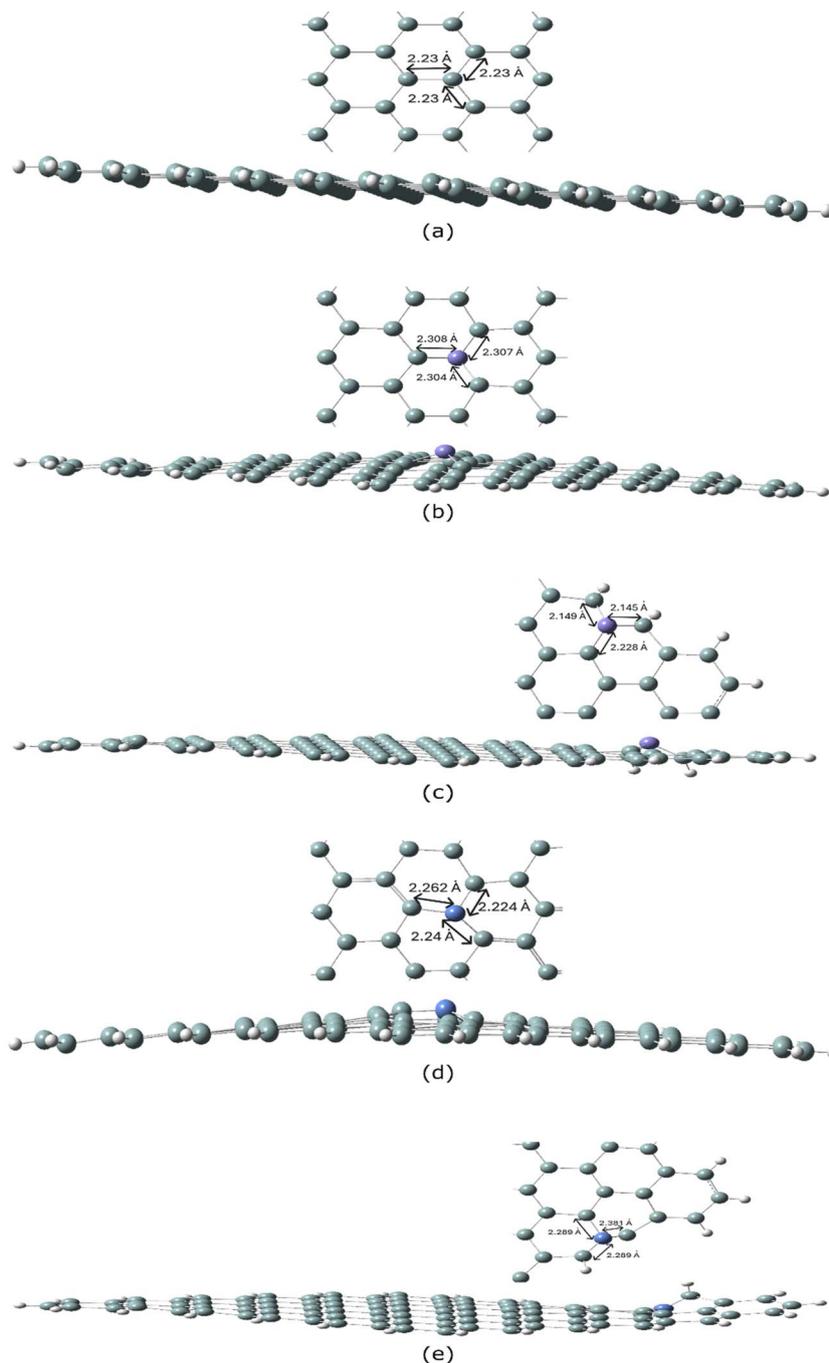
Fig. 2 Optimized structure of the pristine and iron and nickel – doped silicene sheet. The structures include (a) for P–Si, (b) for (Si–Fe–C), (c) for (Si–Fe–E), (d) for (Si–Ni–C), and (e) for (Si–Ni–E).

molecules present on the outer membrane of deceased or deteriorating cells, as well as certain categories of bacteria. This interaction triggers the activation of the complement system through the C1q complex. This kind of activation results in opsonization and augments phagocytosis by macrophages, hence playing a pivotal part in the body's innate immune response. Elevated levels of CRP are associated with a higher likelihood of experiencing cardiovascular events, such as heart attack and stroke.[36] It is regarded as a predictive indicator for cardiovascular disorders.

CRP levels can be quantified by different immunoassays, including enzyme-linked immunosorbent assays (ELISA), immunoturbidimetric assays, and high-sensitivity CRP (hs-CRP) tests. The hs-CRP test is highly valuable for evaluating cardiovascular risk, as it can accurately identify lower levels of CRP with enhanced accuracy. The usual range for C-reactive protein (CRP) levels in the blood is below 3 mg L^{-1}. Levels ranging from 3 mg L^{-1} to 10 mg L^{-1} indicate mild inflammation, whereas levels over 10 mg L^{-1} indicate substantial inflammation caused by either an acute infection or a chronic inflammatory condition.[37] The goal of

advancements in biosensor technology is to create more precise and efficient techniques for detecting CRP, which can help in the early diagnosis and improved treatment of inflammatory disorders. Integrating nanomaterials, like silicene, into CRP biosensors can potentially enhance the sensitivity, specificity, and speed of detection.

Fig. 1(a) represents the molecular structure of human CRP molecule obtained from PDB data. (b) displayed the Molecular Potential Surface (MEP)of CRP molecule, the red regions represent areas of negative electrostatic potential, indicating regions where electron density is high. These regions are typically nucleophilic and attract positively charged species (electrophiles). The blue regions represent areas of positive electrostatic potential, indicating regions where electron density is low. These regions are typically electrophilic and attract negatively charged species (nucleophiles).The shades of yellow and green neutral in terms silicene of electrostatic interactions. MEP maps are invaluable for understanding the charge distribution within a molecule and predicting its reactivity and interactions.[38] HOMO and LUMO maps are often depicted as three-dimensional isosurfaces superimposed on the molecular structure. In Fig. 1(c) represents the electron donor sites, areas where the HOMO is densely populated are potential sites for electron donation in reactions. HOMO is localized around a particular part of the molecule is likely to be more reactive. In Fig. 1(d) represents the electron acceptor sites, areas where the LUMO is concentrated are potential sites for electron acceptance. The LUMO is localized around a specific part of the molecule (as shown in red and green colour), that region is more likely to interact with nucleophiles.[39]

Optimised structure of iron and nickel doped silicene sheets

Fig. 2 shows the optimized structures of pristine (P–Si) and a silicene sheet doped with an iron/nickel atom at both central and peripheral positions. The optimized pristine silicene sheet has a buckling height of 0.43 Å. The bond lengths for Si–Si and Si–H range from 2.23 Å to 2.25 Å and 1.48 Å, respectively and the Si–Si–Si bond angle is 116°. These calculated values are in good agreement with the findings reported in prior research.[40,41] The incorporation of a metal atom into the silicene sheet leads to structural deformation, which can be attributed to the substantial disparity in atomic radii between silicon and the dopants (iron & nickel).

The mean bond lengths for the transition metal-doped silicene sheets were calculated to assess the structural stability and bonding environment around the dopant atoms. For iron-doped silicene, the average bond length was found to be 2.31 Å when doped at the center and 2.17 Å at the edge. In the case of nickel doping, the mean bond lengths were 2.24 Å and 2.18 Å at the center and edge positions, respectively. These variations in bond lengths reflect the influence of dopant type and position on the silicene lattice geometry and may affect the adsorption and sensing performance of the material. Unlike the periodic buckling observed in pristine silicene, the doped structures display uneven buckling due to variations in bond lengths and bond angles. These deformations are primarily caused by the

Table 1 The calculated formation energy (eV), E_{HOMO} (eV), E_{LUMO} (eV), Fermi energy (eV), and energy gap (eV) of pristine and nickel-doped silicene sheets

System	E_{form}	E_{HOMO}	E_{LUMO}	E_F	E_g
Si–Fe–C	−1.73	−4.55	−4.33	−4.44	0.22
Si–Fe–E	−1.42	−4.58	−4.39	−4.48	0.19
Si–Ni–C	−2.35	−4.5	−4.34	−4.42	0.17
Si–Ni–E	−1.49	−4.61	−4.43	−4.52	0.19

differences in atomic radii between silicon and the dopant atoms. The covalent radii of the involved atoms are as follows: silicon (1.11 Å), iron (1.32 Å), and nickel (1.24 Å), as the atomic size of the dopant directly influences the local bonding environment and structural distortion in the silicene sheet.[42]

The introduction of larger transition metal atoms into the silicene lattice leads to local distortion, particularly in the vicinity of the dopant site. Central doping generally results in slightly longer bond lengths compared to edge doping due to the symmetrical distribution of strain and the accommodation of larger atoms within the hexagonal framework. This deformation enhances the chemical activity of the silicene sheet, which positively influences molecule adsorption. The variations in bond angles and lengths induced by metal doping are beneficial for improving the material's reactivity and potential applications in sensor technology.

Formation energy quantifies the energy change associated with the formation of a compound or a structure from its constituent elements in their standard states. It is a measure of the stability of the material, indicating whether the formation of the material is energetically favorable or unfavorable. A negative formation energy value indicates that the formation of the material is exothermic and thus thermodynamically stable.[43]

The formation energy formula to determine the structural stability is

$$E_{form} = E_{P-Si} - \mu_{silicon} + \mu_{dopant} - E_{M-Si} \qquad (5)$$

where E_{form}, E_{P-Si}, $\mu_{silicon}$, and μ_{dopant} and E_{M-Si} stand for the formation energy, the optimized energy of pristine silicene, chemical potential of silicon, dopant atom (Fe/Ni) and the optimized energy of metal doped silicene sheet respectively.

The formation energy values obtained and presented in Table 1 indicate that the inclusion of Fe and Ni as a dopant in the silicene sheet. This suggests that the doping of Fe/Ni atom exhibits good stability, with a negative formation energy.[44] When Fe/Ni replaces a central Si atom, refer Fig. 2(b) and (d) it disrupts the uniform bonding and introduces localized d-orbitals, altering the band structure and potentially creating new electronic states near the HOMO level (refer Table 1), thereby modifying the energy gap. In contrast, replacing an edge Si by Fe/Ni atom as shown in Fig. 2(c) and (e) results in a weaker perturbation due to the already asymmetric bonding environment and fewer neighboring Si atoms, leading to a different impact on the energy gap (E_g).
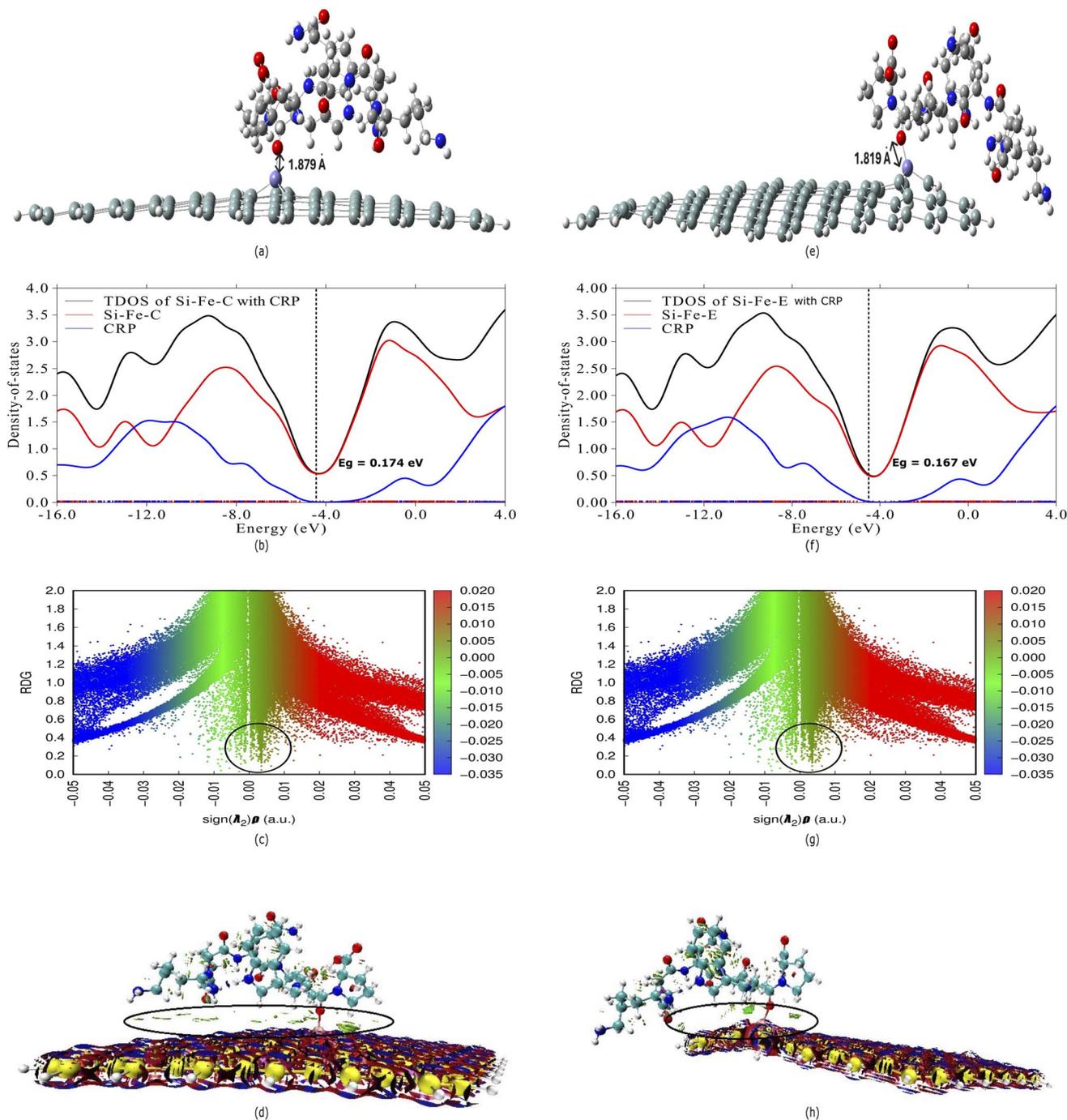
Fig. 3   CRP adsorption on iron-doped silicene: (a and e)-optimized structures, (b and f)-density of states (DOS) plots, (c and g)-reduced density gradient (RDG) analysis, and (d and h)-isosurface charge density maps of CRP adsorbed on iron-doped silicene at central (Si–Fe–C) and edge (Si–Fe–E) sites.

Interaction of iron doped silicene with CRP

The interaction of CRP with iron-doped silicene was investigated for two configurations: iron doped at the center (Si–Fe–C) and at the edges (Si–Fe–E) of the silicene sheet as shown in Fig. 3(a) and (d). The optimized structures revealed strong binding between the doped silicene and CRP, with binding distances of 1.879 Å and 1.819 Å for the central and edge-doped systems, respectively. The adsorption energy plays a crucial role in influencing the efficiency and recyclability of a sensor.

The optimal adsorption energy range is determined by finding the right balance between a sufficiently strong interaction for detection and a weak enough interaction for simple desorption, thereby allowing the sensor to be reused. The adsorption energy must be sufficiently negative to permit effective binding of the target molecule to the sensor surface,

Table 2 Adsorption energies, thermodynamic parameters, and electronic properties of CRP-adsorbed on Si–Fe–C and Si–Fe–E configurations

Parameters	Si–Fe–C with CRP	Si–Fe–E with CRP
ΔE in eV	−1.876	−1.437
ΔH in eV	−1.818	−1.377
ΔG in eV	−1.110	−0.776
ΔS in eV	−0.002	−0.002
Binding distance – d in Å	1.879	1.819
E_{HOMO} in eV	−4.436	−4.491
E_{LUMO} in eV	−4.261	−4.324
E_g in eV	**0.174**	**0.167**
E_F in eV	−4.349	−4.408
$\%\Delta E_g$	**25.584**	**13.820**
Charge transfer e	0.302	0.272

hence enabling reliable detection. The corresponding adsorption energies were calculated to be −1.876 eV for Si–Fe–C and −1.437 eV for Si–Fe–E, as shown in Table 1 indicating that both configurations exhibit favorable and stable adsorption, with the central doping showing slightly stronger interaction.

In order to guarantee the reusability and optimal performance of a sensor, it is crucial to take into account the thermodynamic parameters: enthalpy (ΔH), Gibbs free energy (ΔG), and entropy (ΔS). These parameters offer a thorough comprehension of the stability, spontaneity, and temperature sensitivity of the adsorption process. Enthalpy change (ΔH) quantifies the amount of heat that is either absorbed or emitted during adsorption. Negative (ΔH) indicates an exothermic process where heat is emitted, which usually promotes adsorption. The Gibbs free energy change (ΔG) signifies the inherent tendency of the adsorption process to occur spontaneously. The concept of ΔG combines the changes in enthalpy and entropy, resulting in a negative value represents the spontaneous process that is essential for efficient adsorption.[45] Entropy change (ΔS) quantifies the level of disorder or randomness linked to the adsorption process. A positive ΔS indicates an increase in entropy, which can be advantageous for adsorption operations and a negative ΔS change indicates that the system becomes more organized upon adsorption, which result in increased difficulty in desorption. For Si–Fe–C and Si–Fe–E sheets interacts with CRP produced the negative enthalpy, negative Gibbs free energy and negative entropy values as displayed in the Table 2. Nevertheless, due to the negative value of ΔG, the process continues to occur spontaneously, and desorption may still be possible by implementing controlled circumstances such as adjusting the temperature.

Electronic property analysis revealed a notable reduction in the HOMO–LUMO energy gap upon CRP adsorption. For Si–Fe–C, the energy gap decreased to 0.174 eV (a 25.58% reduction), while for Si–Fe–E, the gap decreased to 0.167 eV (a 13.82% reduction). This decrease in energy gap implies an increase in electrical conductivity and reactivity, which are desirable features for sensor applications. The larger gap reduction in the centrally doped system indicates a more significant electronic

response, suggesting it as a more promising candidate for CRP detection.

Fig. 3(b) and (f) illustrate the Density of States (DOS) plots of the Si–Fe–C and Si–Fe–E sheets following the adsorption of CRP. These plots reveal significant changes in the HOMO and the LUMO levels, indicative of reduced energy gaps and enhanced interaction between the CRP molecule and the doped silicene sheets. Prior to CRP adsorption, the HOMO and LUMO energy levels for the Si–Fe–C sheet were −4.55 eV and −4.33 eV, respectively, while those for Si–Fe–E were −4.58 eV and −4.39 eV (refer Table 1). Upon CRP adsorption, the Si–Fe–C sheet exhibited a stabilization of the HOMO level at −4.44 eV, while the LUMO level decreased to −4.49 eV, resulting in a reduced HOMO–LUMO gap of 0.174 eV representing an approximately 26% variation. In contrast, the Si–Fe–E sheet showed HOMO and LUMO levels at −4.26 eV and −4.32 eV (refer Table 2), respectively, corresponding to a slight decrease in the energy gap by about 14%. This shift in electronic states, especially the pronounced changes observed in the Si–Fe–C sheet, is attributed to significant charge redistribution following the CRP adsorption. Moreover, the frontier molecular orbital distributions confirm that both the HOMO and LUMO densities are predominantly localized on the CRP molecule, highlighting strong charge transfer interactions. These findings indicate that CRP adsorption significantly modifies the electronic properties of doped silicene, thereby validating its potential utility as a sensitive material for bio sensing applications.

To further investigate the electronic behavior of the iron-doped silicene sheets upon interaction with the CRP molecule, the Global Electron Density Transfer (GEDT) was calculated as described by.[46] The GEDT is defined by the equation:

$$\text{GEDT} = -\sum q_A \qquad (6)$$

where q_A represents the net Natural Bond Orbital (NBO) charge, summed over all atoms in the dipolar system. This metric quantifies the extent of charge transfer between interacting species. In the present study, the GEDT values were obtained by calculating the difference in charge concentration of the doped silicene sheets before and after CRP adsorption.

The results, summarized in Table 2, indicate a notable charge transfer from the silicene sheets to the CRP molecule. The Si–Fe–C configuration exhibited the highest net charge transfer of approximately 0.302e, followed by the Si–Fe–E configuration with a value of 0.272e. These positive GEDT values confirm that electrons were transferred from the iron-doped silicene surfaces to the CRP molecule. The magnitude of this charge transfer is a key parameter in evaluating sensor performance, as higher charge transfer typically enhances the sensing response. The substantial electron transfer observed in both center and edge-doped configurations strongly suggests that these systems possess significant sensitivity towards CRP detection.

The nature, type, location, and strength of interactions between the CRP molecule and transition metal-doped silicene sheets were further elucidated using non-covalent interaction
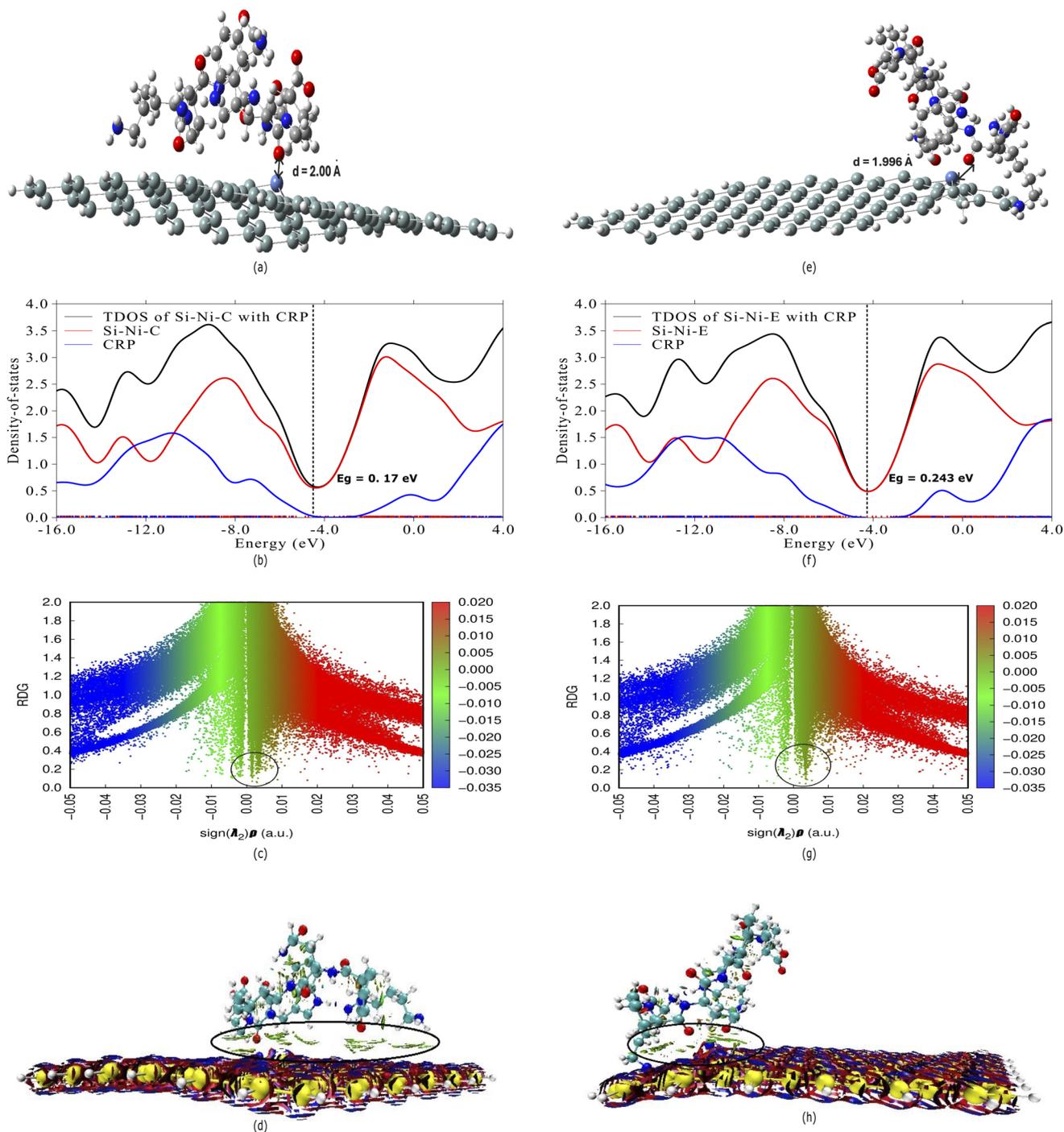
Fig. 4 CRP adsorption on nickel-doped silicene: (a and e)-optimized structures, (b and f)-density of states (DOS) plots, (c and g)-reduced density gradient (RDG) analysis, and (d and h)-isosurface charge density maps of CRP adsorbed on nickel-doped silicene at central (Si–Ni–C) and edge (Si–Ni–E) sites.

(NCI) analysis. To visually interpret these intra- and intermolecular interactions, Reduced Density Gradient (RDG) analysis was employed. The RDG and its corresponding gradient isosurfaces were calculated using the following expression:[47]

$$\text{RDG}(r) = \frac{1}{2(3\pi^2)^{1/3}} \frac{|\nabla \rho(r)|}{\rho(r)^{4/3}} \quad (7)$$

where $\rho(r)$ is the total electron density and $\nabla \rho(r)$ is its gradient. According to Bader's Atoms in Molecules (AIM) theory,[48] the nature of these interactions can be described through the sign of the second largest eigenvalue λ_2 of the Hessian matrix of electron density, expressed as:

$$\Omega(r) = \text{Sign}\,(\lambda_2(r))\,\rho(r) \quad (8)$$

This function, $(\lambda_2(r))\rho(r)$, is instrumental in differentiating interaction types: negative values indicate attractive interactions (*e.g.*, hydrogen bonding), while positive values correspond to repulsive steric effects. Color-coded isosurfaces were used to visually represent these regions—green for van der Waals (vdW) interactions, blue for strong attractive interactions such as hydrogen bonding, and red for repulsive interactions. Fig. 3(c) and (g) display the RDG scatter plots for iron-doped silicene sheets with CRP adsorbed at central and edge doping sites, respectively. Distinct spikes in the range of 0.00 to 0.02 a.u. on the *x*-axis of the scatter plots, marked by green regions within black circles, confirm the presence of vdW interactions. These correspond to non-covalent contacts between the CRP molecule and the silicene surface.[49] Corresponding gradient isosurface plots in Fig. 2(d) and (h) further highlight these interactions. Green, plate-like regions enclosed in black circles are indicative of vdW interactions occurring primarily between the oxygen atoms of the CRP molecule and the iron-doped region of the silicene. Additionally, blue regions observed around the doped iron atoms on the silicene sheet suggest the presence of hydrogen bonding between silicon and the transition metal dopant. Overall, RDG analysis reveals that vdW forces dominate the interaction between CRP and iron-doped silicene, supported by both real-space isosurface visualization and the distribution of sign $(\lambda_2)\rho$ values. These findings provide crucial insight into the physical adsorption mechanism and its relevance to biosensing performance.

Interaction of nickel doped silicene with CRP

Fig. 4 presents the optimized geometries of nickel-doped silicene interacting with the CRP molecule, with doping performed at both the center (Si–Ni–C) and edge (Si–Ni–E) positions. In both configurations, the interaction predominantly occurs between the nickel dopant site and the oxygen atom of the CRP molecule. The shortest intermolecular distances were found to be 2.01 Å for the Si–Ni–C system and 1.996 Å for the Si–Ni–E system. These relatively short contact distances suggest strong physical interactions between the doped silicene surface and the CRP molecule. The slight reduction in intermolecular distance at the edge-doped site indicates marginally stronger

interaction compared to center doping. This close proximity facilitates effective charge redistribution, which is a critical factor in enhancing the sensitivity of the material.

An optimal reusable sensor should preferably have an adsorption energy ranging from −0.5 to −1.0 eV.[50] This range strikes a balance between effective detection and ease of desorption, ensuring the sensor can be used multiple times without significant degradation or loss of sensitivity. In this context, the interaction of the Si–Ni–C configuration with the CRP molecule yields an adsorption energy of −0.7216 eV, while the Si–Ni–E configuration results in a significantly stronger interaction with an adsorption energy of −1.82 eV, as presented in Table 3. The adsorption energy for the Si–Ni–C system falls squarely within the optimal range, suggesting that this configuration enables effective CRP detection while maintaining the potential for reusability. Conversely, the significantly stronger binding observed in the Si–Ni–E system indicates a high sensitivity toward CRP detection; however, such strong interaction may impede desorption of the analyte, thereby limiting the sensor's suitability for repeated or long-term use.

The interaction of CRP with Si–Ni–C and Si–Ni–E sheets reveals significant differences in adsorption behavior and thermodynamic stability. For the Si–Ni–C–CRP system, the adsorption energy of −0.72 eV along with negative enthalpy indicates an exothermic interaction, suggesting that the process releases energy. However, the positive Gibbs free energy implies that the adsorption is not spontaneous under standard conditions, possibly due to an accompanying decrease in entropy, as indicated by the negative entropy value. This reduction in disorder might be due to restricted molecular motion upon adsorption. In contrast, the Si–Ni–E–CRP interaction, with a more negative adsorption energy of −1.82 eV and both negative enthalpy and Gibbs free energy, suggests a strongly exothermic and spontaneous adsorption process. The negative entropy again indicates a decrease in disorder, but the spontaneity here reflects a thermodynamically favorable interaction, likely due to stronger binding or better electronic compatibility between CRP and the Si–Ni–E sheet.

The interaction of CRP with Si–Ni–C and Si–Ni–E sheets can be comprehensively understood through the combined analysis of adsorption energy, thermodynamic parameters, density of states (DOS), energy gap variation, and NBO charge transfer. The NBO analysis reveals a charge transfer of 0.182*e* from CRP to the Si–Ni–C sheet, whereas a significantly higher transfer of 0.322*e* occurs in the case of the Si–Ni–E sheet. This greater charge exchange in the Si–Ni–E with CRP system indicates a stronger electronic interaction and more effective sensing behavior.[51] Additionally, the HOMO–LUMO gap of Si–Ni–E increases from 0.185 eV to 0.243 eV upon CRP adsorption, as supported by the DOS plots in Fig. 4(b) and (f). This notable widening of the band gap indicates a stronger perturbation in the electronic structure, signifying a higher degree of interaction and charge transfer between CRP and the Si–Ni–E sheet.

The DOS plots reinforce this observation, where the total DOS (black line) shows more pronounced changes near the Fermi level for the Si–Ni–E with CRP system. In contrast, the Si–Ni–C sheet shows only a minor change in band gap (from

Table 3 Adsorption energies, thermodynamic parameters, and electronic properties of CRP-adsorbed Si–Ni–C and Si–Ni–E configurations

Parameters	Si–Fe–C with CRP	Si–Fe–E with CRP
ΔE in eV	−0.7216	−1.819
ΔH in eV	−0.672	−1.750
ΔG in eV	0.634	−1.015
ΔS in eV	−0.004	−0.002
Binding distance – d in Å	2.010	1.996
E_{HOMO} in eV	−4.506	−4.277
E_{LUMO} in eV	−4.335	−4.033
E_g in eV	**0.170**	**0.244**
E_F in eV	−4.420	−4.155
%ΔE_g	**1.279**	**24.023**
Charge transfer e	0.182	0.322

0.168 eV to 0.17 eV), consistent with its lower charge transfer and weaker interaction. These results, along with the more negative adsorption energy and favorable thermodynamic properties of the Si–Ni–E with CRP system, confirm that Si–Ni–E exhibits a superior affinity and enhanced sensitivity for CRP detection compared to Si–Ni–C.

As previously discussed, the nature, type, location, and strength of interactions between the CRP molecule and nickel doped silicene sheets were further investigated through non-covalent interaction analysis. The RDG scatter plots for Si–Ni–C and Si–Ni–E with CRP displays here with distinct spikes in the range of 0.00 to 0.02 a.u. highlighted by green regions within black circles, which confirm the presence of vdW interactions. Complementary isosurface plots shown in Fig. 4(d) and (h) further illustrate these interactions, with green, plate-like regions—again circled in black—indicating vdW forces predominantly occurring between the oxygen atoms of the CRP molecule and the nickel-doped areas of the silicene sheets. Overall, the RDG analysis clearly demonstrates that van der Waals interactions are the dominant force governing the CRP–silicene interaction.

Conclusion

In this study, we explored the bio sensing potential of iron and nickel doped silicene with dopants positioned at central and edge sites for the detection of C-reactive protein (CRP), using density functional theory calculations at the B3LYP level in Gaussian 16. Iron and Nickel-doped silicene demonstrates significant thermodynamic stability as indicated by its negative formation energy. This stability is critical for the robustness and durability of the sensor in various conditions.

Our comprehensive analysis, including adsorption energetics, thermodynamic behavior, electronic structure modulation, density of states, and non-covalent interaction plots, reveals that doping significantly enhances the sensitivity of silicene toward CRP. Among the studied configurations, Fe-doped silicene at the central site (Si–Fe–C) exhibited the strongest interaction with CRP, with high adsorption energy (−1.876 eV), favorable thermodynamic parameters, substantial charge transfer (0.302e), and a significant reduction in the HOMO–LUMO gap (25.6%), all indicating strong sensor responsiveness. Similarly, Ni-doped silicene at the edge site (Si–Ni–E) demonstrated excellent sensing performance with an adsorption energy of −1.819 eV and a 24.0% energy gap change. DOS and NCI analyses further confirmed the enhanced reactivity and non-covalent stabilization of CRP on the doped surfaces. These findings demonstrate that strategic doping of silicene with transition metals not only improves its binding affinity toward CRP but also leads to measurable changes in electronic properties, making doped silicene a promising candidate for next-generation 2D bio sensing platforms.

Conflicts of interest

There are no conflicts to declare.

Data availability

No primary research results, software or code have been included and no new data were generated or analysed as part of this review.

Acknowledgements

References

1 A. K. Shrivastava, H. V. Singh, A. Raizada and S. K. Singh, C-reactive protein, inflammation and coronary heart disease, *Egypt. Heart J.*, 2015, **67**(2), 89–97.

2 I. Letchumanan, M. K. M. Arshad and S. C. B. Gopinath, Nanodiagnostic attainments and clinical perspectives on C-reactive protein: cardiovascular disease risks assessment, *Curr. Med. Chem.*, 2021, **28**(5), 986–1002.

3 H. Sohrabi, H. K. Kordasht, P. Pashazadeh-Panahi, P. Nezhad-Mokhtari, M. Hashemzaei, M. R. Majidi, J. Mosafer, F. Oroojalian, A. Mokhtarzadeh and M. D. L. Guardia, Recent advances of electrochemical and optical biosensors for detection of C-reactive protein as a major inflammatory biomarker, *Microchem. J.*, 2020, **158**, 105287.

4 A. Haleem, M. Javaid, R. P. Singh, R. Suman and S. Rab, Biosensors applications in medical field: A brief review, *Sens. Int.*, 2021, **2**, 100100.

5 R. Keçili, S. Büyüktiryaki and C. M. Hussain, Advancement in bioanalytical science through nanotechnology: past, present and future, *TrAC, Trends Anal. Chem.*, 2019, **110**, 259–276.

6 J. Wang and X. Qu, Recent progress in nanosensors for sensitive detection of biomolecules, *Nanoscale*, 2013, **5**(9), 3589–3600.

7 K. Khan, A. Khan Tareen, M. Aslam, R. Wang, Y. Zhang, A. Mahmood, Z. Ouyang, H. Zhang and Z. Guo, Recent developments in emerging two-dimensional materials and their applications, *J. Mater. Chem. C*, 2020, **8**(2), 387–440.

8 A. Gupta, T. Sakthivel and S. Seal, Recent development in 2D materials beyond graphene, *Prog. Mater. Sci.*, 2015, **73**, 44–126.

9 H. Lin, W. Qiu, J. Liu, L. Yu, S. Gao, H. Yao, Y. Chen and J. Shi, Silicene: wet-chemical exfoliation synthesis and biodegradable tumor nanomedicine, *Adv. Mater.*, 2019, **31**(37), 1903013.

10 Y. You, C. Yang, X. Zhang, H. Lin and J. Shi, Emerging two-dimensional silicene nanosheets for biomedical applications, *Mater. Today Nano*, 2021, **16**, 100132.

11 R. Hu, Z. Chen, D. Chen, X. Guo, W. Feng, Z. Liu, H. Lin, Y. Chen and R. Wu, Engineering two-dimensional silicene composite nanosheets for dual-sensitized and photonic hyperthermia-augmented cancer radiotherapy, *Biomaterials*, 2021, **269**, 120455.

12 K. Devi and K. K. Singh, Enhancing the Glucose Sensing Properties of Silicene Through Transition Metal Doping: a DFT Investigation, *Adv. Theory Simul.*, 2024, 2400166.

13 G. R. Bhimanapati, L. Zhong, M. Vincent, Y. Jung, J. Cha, S. Das, D. Xiao, *et al.*, Recent advances in two-dimensional materials beyond graphene, *ACS Nano*, 2015, **9**(12), 11509–11539.

14 M. Ge, C. Cao, G. M. Biesold, C. D. Sewell, S.-M. Hao, J. Huang, W. Zhang, Y. Lai and Z. Lin, Recent advances in silicon-based electrodes: from fundamental research toward practical applications, *Adv. Mater.*, 2021, **33**(16), 2004577.

15 W. Tao, N. Kong, X. Ji, Y. Zhang, A. Sharma, J. Ouyang, B. Qi, *et al.*, Emerging two-dimensional monoelemental materials (Xenes) for biomedical applications, *Chem. Soc. Rev.*, 2019, **48**(11), 2891–2912.

16 M. M. Korah, T. Nori, S. Tongay and M. D. Green, Harnessing biological applications of quantum materials: opportunities and precautions, *J. Mater. Chem. C*, 2020, **8**(31), 10498–10525.

17 I. Gablech, J. Pekárek, J. Klempa, V. Svatoš, A. Sajedi-Moghaddam, P. Neužil and M. Pumera, Monoelemental 2D materials-based field effect transistors for sensing and biosensing: phosphorene, antimonene, arsenene, silicene, and germanene go beyond graphene, *TrAC, Trends Anal. Chem.*, 2018, **105**, 251–262.

18 S. Ghosal, A. Bandyopadhyay, S. Chowdhury and D. Jana, A review on transport characteristics and Bio-sensingapplication of Silicene, *Rep. Prog. Phys.*, 2023, **86**(9), 096502.

19 Y. Qian and H. Yang, Computational insight into the bioapplication of 2D materials: A review, *Nano Today*, 2023, **53**, 102007.

20 K. devi Pethurajan and K. K. Singh, A DFT studies on absorbing and sensing possibilities of glucose on graphene surface doped with Ag, Au, Cu, Ni & Pt atoms, *Biosens. Bioelectron.: X*, 2023, **13**, 100287.

21 (*a*) A. D. Becke, *Phys. Rev. A*, 1993, **38**, 3098; (*b*) A. D. Becke, *J. Chem. Phys.*, 1988, **98**, 1372; (*c*) A. D. Becke, Density–functional thermochemistry. III. The role of exact exchange, *J. Chem. Phys.*, 1993, **98**(7), 5648–5652.

22 P. J. Hay and W. R. Wadt, Ab initio effective core potentials for molecular calculations. Potentials for K to Au including the outermost core orbitals, *J. Chem. Phys.*, 1985, **82**(1), 299–310.

23 Y. Yang, M. N. Weaver and K. M. Merz Jr., Assessment of the "6-31+ G** + LANL2DZ" mixed basis set coupled with density functional theory methods and the effective core potential: prediction of heats of formation and ionization potentials for first-row-transition-metal complexes, *J. Phys. Chem. A*, 2009, **113**(36), 9843–9851.

24 K. Pethurajan and K. K. Singh, Electronic and work function-based glucose sensors on graphene, silicene, and germanene sheets–DFT studies, *Comput. Theor. Chem.*, 2023, **1225**, 114134.

25 R. Chandiramouli, A. Srivastava and V. Nagarajan, NO adsorption studies on silicene nanosheet: DFT investigation, *Appl. Surf. Sci.*, 2015, **351**, 662–672.

26 J. W. Ochterski, *Thermochemistry in Gaussian*, Gaussian Inc, 2000, vol. 1, pp. 1.

27 M. J. Frisch, G. W. Trucks, H. B. Schlegel, G. E. Scuseria, M. A. Robb, J. R. Cheeseman, G. Scalmani, V. Barone, G. A. Petersson, H. Nakatsuji, X. Li, M. Caricato, A. V. Marenich, J. Bloino, B. G. Janesko, R. Gomperts, B. Mennucci, H. P. Hratchian, J. V. Ortiz; A. F. Izmaylov, J. L. Sonnenberg, D. Williams-Young, F. Ding, F. Lipparini, F. Egidi, J. Goings, B. Peng, A. Petrone, T. Henderson, D. Ranasinghe, V. G. Zakrzewski, J. Gao, N. Rega, G. Zheng, W. Liang, M. Hada, M. Ehara, K. Toyota, R. Fukuda, J. Hasegawa, M. Ishida, T. Nakajima, Y. Honda, O. Kitao, H. Nakai, T. Vreven, K. Throssell, J. A. Jr. Montgomery, J. E. Peralta, F. Ogliaro; M. J. Bearpark, J. J. Heyd, E. N. Brothers, K. N. Kudin, V. N. Staroverov, T. A. Keith, R. Kobayashi, J. Normand, K. Raghavachari, A. P. Rendell, J. C. Burant, S. S. Iyengar, J. Tomasi, M. Cossi, J. M. Millam, M. Klene, C. Adamo, R. Cammi, J. W. Ochterski, R. L. Martin, K. Morokuma, O. Farkas, J. B. Foresman and D. J. Fox, *Gaussian 16 Revision C.01*, Gaussian, Inc., Wallingford CT, 2016.

28 K. Pethurajan and K. K. Singh, A DFT studies on absorbing and sensing possibilities of glucose on graphene surface doped with Ag, Au, Cu, Ni & Pt atoms, *Biosens. Bioelectron.: X*, 2023, **13**, 100287.

29 F. Weinhold, C. R. Landis and E. D. Glendening, What is NBO analysis and how is it useful?, *Int. Rev. Phys. Chem.*, 2016, **35**(3), 399–440.

30 V. Nagarajan and R. Chandiramouli, Investigation on adsorption properties of CO and NO gas molecules on aluminene nanosheet: a density functional application, *Mater. Sci. Eng., B*, 2018, **229**, 193–200.

31 P. K. Devi and K. K. Singh, Improving the electronic and optical properties of silicene by doping with transition metals–A DFT investigation, *Comput. Theor. Chem.*, 2025, 115117.

32 M. J. Szary, Toward high selectivity of sensor arrays: Enhanced adsorption interaction and selectivity of gas detection (N2, O2, NO, CO, CO2, NO2, SO2, AlH3, NH3, and PH3) on transition metal dichalcogenides (MoS2, MoSe2, and MoTe2), *Acta Mater.*, 2024, **274**, 120016.

33 R. A. Boto, J.-P. Piquemal and J. Contreras-García, Revealing strong interactions with the reduced density gradient: a benchmark for covalent, ionic and charge-shift bonds, *Theor. Chem. Accounts Theor. Comput. Model.*, 2017, **136**, 139.

34 N. R. Sproston and J. A. Jason, Role of C-reactive protein at sites of inflammation and infection, *Front. Immunol.*, 2018, **9**, 754.

35 L. A. Potempa, B. A. Maldonado, P. Laurent, E. S. Zemel and H. Gewurz, Antigenic, electrophoretic and binding alterations of human C-reactive protein modified selectively in the absence of calcium, *Mol. Immunol.*, 1983, **20**(11), 1165–1175.

36 Emerging Risk Factors Collaboration, C-reactive protein concentration and risk of coronary heart disease, stroke, and mortality: an individual participant meta-analysis, *Lancet* 375, 9709, 2010, 132–140.

37 T. A. Pearson, G. A. Mensah, R. W. Alexander, J. L. Anderson, R. O. Cannon III, M. Criqui and Y. Y. Fadl, Markers of inflammation and cardiovascular disease: application to clinical and public health practice: a statement for healthcare professionals from the Centers for Disease Control and Prevention and the American Heart Association, *Circulation*, 2003, **107**(3), 499–511.

38 D. P. L. Renj, R. Racil Jeya Geetha, A. Benifa, M. Amalanathan, M. Sony Michael Mary, Z. Ratković, J. Muškinja and J. Micheal, Density functional theory calculations, vibrational spectral analysis and topological analysis of 1-acethy-2 (4-isopropoxy-3-methoxyphenyl) cyclopropane with docking studies, *Chem. Phys. Impact*, 2024, **8**, 100524.

39 J. Borges Itamar, R. S. S. Oliveira, M. A. S. Oliveira, Properties of molecular charge distributions affecting the sensitivity of energetic materials, *Theoretical and computational chemistry*, 2022, vol. 22, pp. 81–105.

40 S. Bhai and G. Bishwajit, 2D silicene nanosheets for the detection of DNA nucleobases for genetic biomarker: a DFT study, *Struct. Chem.*, 2024, **35**(1), 25–37.

41 J.-W. Feng, Y.-J. Liu, H.-X. Wang, Z. Jing-xiang, Q.-H. Cai and X.-Z. Wang, Gas adsorption on silicene: a theoretical study, *Comput. Mater. Sci.*, 2014, **87**, 218–226.

42 B. Cordero, V. Gómez, A. E. Platero-Prats, M. Revés, J. Echeverría, E. Cremades, F. Barragán and S. Alvarez, Covalent radii revisited, *Dalton Trans.*, 2008, **21**, 2832–2838.

43 T.-F. Yi, Y. Xie, Y.-R. Zhu, R.-S. Zhu and H. Shen, Structural and thermodynamic stability of Li4Ti5O12 anode material for lithium-ion battery, *J. Power Sources*, 2013, **222**, 448–454.

44 P. Kalpanadevi and K. K. Singh, Enhancement of electronic and optical characteristics of graphene by doping with transition metals–DFT method, *Phys. B*, 2023, **669**, 415309.

45 T. A. Saleh, Kinetic models and thermodynamics of adsorption processes: Classification, *Interface Science and Technology*, 2022, **34**, 65–97.

46 S. A. Siadati, E. Vessally, A. Hosseinian and L. Edjlali, Possibility of sensing, adsorbing, and destructing the Tabun-2D-skeletal (Tabun nerve agent) by C20 fullerene and its boron and nitrogen doped derivatives, *Synth. Met.*, 2016, **220**, 606–611.

47 E. R. Johnson, S. Keinan, P. Mori-Sánchez, J. Contreras-García, A. J. Cohen and W. Yang, Revealing noncovalent interactions, *J. Am. Chem. Soc.*, 2010, **132**(18), 6498–6506.

48 W. Tang, E. Sanville and G. Henkelman, A grid-based Bader analysis algorithm without lattice bias, *J. Phys.: Condens. Matter*, 2009, **21**(8), 084204.

49 T. Aiswarya and K. K. Singh, Incrimination and impact on recovery times and effects of BN nanostructures on antineoplastic drug-electronic density study, *J. Mol. Model.*, 2024, **30**(11), 372.

50 N. T. Nguyen, D. Q. Ho and T. Nguyen Tien, Theoretical insights into the adsorption and gas sensing performance of Fe/Cu-adsorbed graphene, *Phys. Chem. Chem. Phys.*, 2024, **26**(19), 14265–14276.

51 H. Y. Mao, Y. H. Lu, J. D. Lin, S. Zhong, A. T. S. Wee and W. Chen, Manipulating the electronic and chemical properties of graphene *via* molecular functionalization, *Prog. Surf. Sci.*, 2013, **88**(2), 132–159.